

Spin and reoccupation noise beyond the fluctuation-dissipation theorem

Julia Wiegand,¹ Dmitry S. Smirnov,² Jens Hübner,^{1,*} Mikhail M. Glazov,² and Michael Oestreich^{1,†}

¹*Institut für Festkörperphysik, Leibniz Universität Hannover, Appelstraße 2, D-30167 Hannover, Germany*

²*Ioffe Institute, Polytechnicheskaya 26, 194021 St. Petersburg, Russia*

(Dated: June 13, 2022)

We report on the non-equilibrium spin noise of a single InGaAs quantum dot charged by a single hole under strong driving by a linearly polarized probe light field. The spectral dependency of the spin noise power evidences a pure homogeneous broadening and negligible charge fluctuation in the environment of the unbiased quantum dot. Full analysis of the spin noise spectra beyond the fluctuation-dissipation theorem yields the heavy-hole spin dynamics as well as the trion spin dynamics. Additionally the experiment reveals a novel, much weaker spin noise contribution observed at the quantum dot resonance showing a significantly longer correlation time. Magnetic-field dependent measurements in combination with theoretical modelling prove that this additional noise contribution unveils a charge reoccupation noise which is intrinsic in naturally charged quantum dots.

The efficient optical spin manipulation of individual two-level systems opens fascinating perspectives for spin-photon interfaces, quantum cryptography, and quantum information processing [1, 2]. One of the particularly promising solid state candidates for such spin-photon quantum devices is a single spin localized in a semiconductor quantum dot (QD). Such a system not only provides very long coherence times and a large spin-photon coupling strength but also controlled tuning of the emission wavelength and of the fine structure splitting. Indeed efficient spin manipulation [3–5], spin detection [6, 7], and generation of highly indistinguishable photon pairs [8–10] were already demonstrated in optimized quantum dot microcavity structures.

The spin dynamics of semiconductor quantum optical systems can be optimally studied by spin noise spectroscopy (SNS) [11] which avoids non-resonant optical excitation. The quantum optical technique has been transferred to semiconductor physics during the last decade [12–17], revealing not only charge and nuclear spin dynamics [18, 19] but also higher-order spin correlators [20, 21]. SNS is mostly used as a weakly interacting, nondestructive measurement technique but spin noise (SN) measurements beyond the fluctuation-dissipation theorem can offer additional information about the coupling and correlation between spin coherences, the response to resonant driving fields, and charging dynamics [22–25]. Lately, the first SN of a single QD was reported [26], where the QD resonance was *inhomogeneously* broadened due to charge fluctuations of residual impurities in the surrounding of the QD [27]. In this work we employ SNS in view of spin-photon interfaces and investigate the spin dynamics of a coherent superposition of a single hole and the corresponding trion state of a *homogeneously* broadened strongly driven QD. The observed dynamics in the coupled QD microcavity system allow us to understand physical limits and challenges of optically driven charged QDs as solid state qubits—one of these challenges being the intrinsic reoccupation noise.

The studied sample comprises a single layer of self-assembled In(Ga)As QDs grown by molecular beam epitaxy on a (001)-oriented GaAs substrate. The QD layer has a gradient in QD density from zero to about 100 dots/ μm^2 . A *p*-type background doping of $\approx 10^{14}$ holes/ cm^3 ensures that a fraction of the QDs is occupied by a single hole. The QDs are embedded in an asymmetric GaAs/AlGaAs Bragg λ -microcavity with an estimated *Q*-factor of ≈ 4000 . The QD microcavity is operating in the weak coupling regime, enhances the light-matter coupling, increases the ratio of SN to optical shot noise, and enables measurements in reflection geometry. The measurement setup is a low-temperature confocal microscope with two detection arms, one for PL analysis and one for SNS (see [26, 28]). The QD sample is cooled down to 4.2 K and, for PL measurements, excited above the QD barrier by a cw diode laser with a photon energy of 1.59 eV. The black solid line in Fig. 1 shows the PL spectrum of a single QD in a sample region of very low QD density. The measured linewidth of the PL does not reflect the natural linewidth of the QD but is limited by the optical excitation power and the spectral resolution of the spectrometer. All results below are measured on this specific QD but control measurements on other QDs yield consistent results. The transition at higher photon energy is attributed to the neutral exciton (X^0) and the transition at lower photon energy to the positively charged trion (X^{1+}) (see [28] for details), which is in good agreement with the QD PL spectra in Ref. [29]. The assignment is confirmed below by spectrally resolved measurements of the SN power.

The SN of the QD is measured by a linearly polarized cw Ti:sapphire ring laser which is stabilized to a Fizeau wavelength meter and focused onto the sample to a spot with a diameter of 1 μm . The fluctuations of the Kerr rotation angle due to spin fluctuations in the single QD are measured by a polarization bridge with a low-noise balanced photo receiver. The resulting electric signal is amplified, digitized, and Fourier transformed in

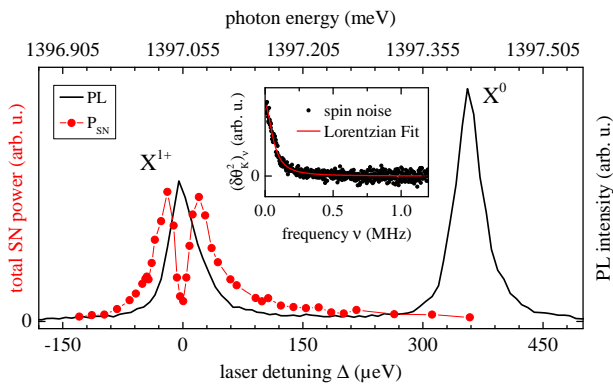


FIG. 1. PL spectrum of the QD showing trion (X^{1+}) and exciton (X^0) transition. The red data points depict the corresponding SN power measured as a function of laser detuning with respect to the trion resonance. The red line is a guide to the eye. The inset shows a typical SN spectrum (black dots) at a detuning of $\Delta = -97 \mu\text{eV}$ with a Lorentzian fit (red line).

real time to obtain a SN frequency spectrum and the SN power, i.e., the integrated SN frequency spectrum. A small longitudinal magnetic field ($B_z = 31 \text{ mT}$) is applied to increase the longitudinal spin relaxation time T_1 and thereby improve the signal-to-noise ratio [26]. A background spectrum acquired in purely transverse magnetic field ($B_x = 27 \text{ mT}$) is subtracted from this SN spectrum to isolate the SN from the noise background of optical shot noise and electrical noise. The small transverse magnetic field efficiently suppresses the SN since the projection of the longitudinal spin component on the direction of detection is strongly reduced and the broad transverse spin component with the transversal spin relaxation time $T_2 \ll T_1$ is negligible in the measured frequency bandwidth.

The red dots in Fig. 1 depict the integrated SN power measured as a function of probe laser detuning Δ with respect to the trion resonance for a laser intensity of $I = 1.1 \mu\text{W}/\mu\text{m}^2$. The distinct shape of the SN power spectrum $P_{SN}(\Delta)$, with two sharp maxima symmetrically around the QD resonance, proves that the QD resonance is homogeneously broadened, i.e., processes usually leading to inhomogeneous broadening in unbiased QDs, such as charge fluctuations in the QD environment [26], play a negligible role for this QD. The inset shows a typical SN frequency spectrum measured for a probe laser energy strongly negatively detuned from the optical resonance by $\Delta = -97 \mu\text{eV}$. This SN spectrum has a Lorentzian line shape and the corresponding half width at half maximum (HWHM) yields the spin correlation rate. In this case the QD excitation is negligible and the HWHM is proportional to the inverse longitudinal heavy-hole spin relaxation time $T_1^h = 1/(2\pi\text{HWHM})$. We find from the Lorentzian fit $T_1^h \approx 2.5 \mu\text{s}$, which evidences efficient decoupling of hole and nuclear spins in the applied

magnetic field [26, 30].

Next, we examine the SN spectra at small detunings. The SN power has a minimum at zero detuning but does not go to zero which seems, at first glance, inconsistent with the SN from a homogeneously broadened two level system. A more detailed investigation of the SN frequency spectra in the quasi-resonant regime reveals (a) an additional noise contribution and (b) the influence of strong coherent excitation of the trion. Figure 2(a) shows the SN spectrum at $9 \mu\text{eV}$ detuning as an example. In addition to the main Lorentzian denoted α (red line), that dominates the SN spectrum at large laser detuning (inset in Fig. 1), we observe a second Lorentzian contribution denoted β (blue line). The second Lorentzian has a significantly smaller width, i.e., a longer correlation time, and a significantly smaller maximal noise power compared to the α -contribution. The respective SN power spectra of the α - and β -contribution are depicted in Fig. 2(b). The SN power spectrum of the α -contribution is in excellent agreement with the expected line shape for the SN of a single hole

$$P_{SN,\alpha}(\Delta) = A \frac{\Delta^2}{(\Gamma^2 + \Delta^2)^2}, \quad (1)$$

where the parameter Γ describes the width of the SN power spectrum (cf. Fig. 2(b)) and A determines the amplitude of the spectrum. Note that strong coherent excitation of the trion results in a much larger Γ than the intrinsic linewidth γ [28, 31]. Indeed, a fit to the data based on Eq. (1), shown by the gray line in Fig. 2(b), yields a value of $17 \mu\text{eV}$ for Γ which is about one order of magnitude larger than the typical γ of self-assembled QDs, in agreement with the model below.

The red dots in Fig. 2(c) show the detuning dependence of the α correlation rate which, for large detunings, is associated with the relaxation of the heavy-hole spin. The rate strongly increases in the vicinity of the trion resonance which proves that trion excitation by the probe laser significantly affects the spin dynamics. The SN power and the correlation rate of the α -contribution closest to zero detuning could not be extracted from the SN spectrum since its SN power decreases towards zero and its Lorentzian width becomes much larger than the detection bandwidth of 1.8 MHz .

The broadening of the SN power spectrum and the increase of the correlation rate of the α -contribution can be readily explained in the framework of a four level system shown in Fig. 3(a). Absorption of a σ^+ or σ^- cavity photon by the QD results in a transition from the hole $|\pm 3/2\rangle$ spin state to the trion $|\pm 1/2\rangle$ state, respectively, as shown by the red arrows. The generation rate is given by [32]

$$G = \frac{\mathcal{E}^2 \gamma}{\gamma^2 + \Delta^2}, \quad (2)$$

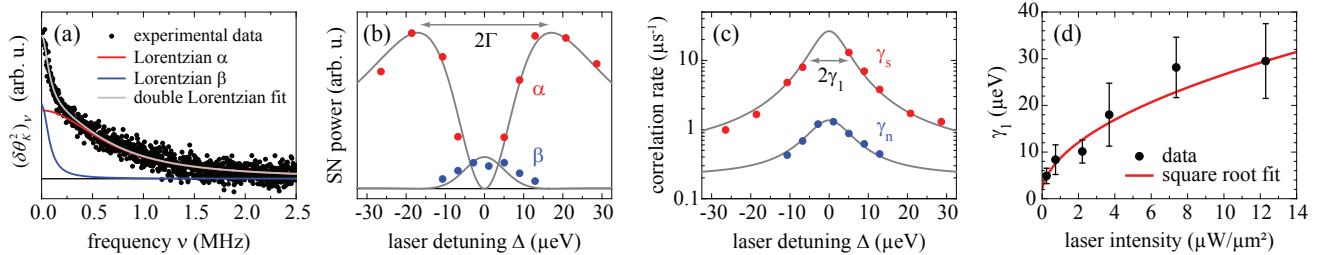


FIG. 2. (a) Typical SN spectrum for a probe laser detuning of $\Delta = 9 \mu\text{eV}$. The spectrum consists of two Lorentzian contributions α and β . (b) SN power spectrum of the α - and β -contribution. The gray lines correspond to a global fit according to Eqs. (1) and (7), respectively. (c) Correlation rates γ_s (α -contribution) and γ_n (β -contribution) as a function of detuning. The gray lines are Lorentzian fits. (d) Intensity dependence of the trion linewidth γ_1 . The red line is a fit according to Eq. (5) describing saturation broadening.

where \mathcal{E} is the matrix element of the trion optical transition, which is proportional to the interband dipole matrix element and the electric field amplitude in the cavity [28]. The transition back to the ground state (blue arrows in Fig. 3(a)) can be induced either by stimulated photon emission or by trion recombination without light emission into the main cavity mode. In the weak coupling regime the trion recombination rate $R = G + \gamma_0$ can be presented as the sum of the generation rate G and the intrinsic recombination rate γ_0 . In addition, nonradiative trion recombination can result in a transition of the hole from the QD into an outer state $|\text{out}\rangle$ via the Auger recombination process with a rate γ_a [31, 33, 34]. The recharging process returns a hole from $|\text{out}\rangle$ back into the QD ground state with a rate γ_r . We will show below that the generation and recombination processes are by a few orders of magnitude faster than the Auger recombination, QD recharging, and spin relaxation processes so that the steady state occupancy of the trion state n_{tr} is determined by the balance of generation and recombination rates

$$n_{\text{tr}} = \frac{G}{G + R} n, \quad (3)$$

with n being the probability to find the QD in the charged state, i.e., occupied by a hole or a trion. The average spin relaxation rate is the weighted sum of spin relaxation rates of the hole in the ground state, $1/T_1^h$, and the electron in the trion, $1/T_1^e$, [24]

$$\gamma_s = \frac{n_h}{n} \frac{1}{T_1^h} + \frac{n_{\text{tr}}}{n} \frac{1}{T_1^e}, \quad (4)$$

where $n_h = n - n_{\text{tr}}$ is the probability that the QD is in the ground state. Taking into account the dependence of the generation rate on the detuning by Eq. (2), one can see that the dependence of γ_s on Δ is described by a Lorentzian, as shown by the gray line in Fig. 2(c). The HWHM of the Lorentzian profile $\gamma_s(\Delta)$ is determined by the trion linewidth [28] and denoted as γ_1 in the following. Fig. 2(d) shows the measured γ_1 as a function of the

probe laser intensity. The measured intensity dependence is perfectly described by saturation broadening [28]

$$\gamma_1(I) = \gamma \sqrt{1 + \frac{I}{I_0}}, \quad (5)$$

where $I/I_0 = 2\mathcal{E}^2/(\gamma\gamma_0)$. The fit of γ_1 according to Eq. 5 is shown as red line in Fig. 2(d) and yields the intrinsic HWHM of the trion transition $\gamma = 2.2 \mu\text{eV}$ and the saturation intensity $I_0 = 0.07 \mu\text{W}/\mu\text{m}^2$. At the same time, the strong increase of the spin relaxation rate γ_s in the vicinity of the trion resonance is related to the fast spin relaxation of the electron in the trion, i.e., the electron spin in the trion relaxes orders of magnitudes faster than the hole spin. The fit of γ_s for different detunings and intensities yields the longitudinal electron-in-trion spin relaxation time $T_1^e \approx 30 \text{ ns}$ (see [28] for details).

Now we proceed to the detailed investigation of the β -component which is characterized by a different dependence on the detuning and a significantly lower correlation rate compared to the α -component. The SN power spectrum of the β -contribution has a maximum at the QD resonance which suggests one of the following origins (see [28]): (i) spin splitting noise, which can be produced by nuclear spin fluctuations [18], (ii) resonance frequency fluctuations due to charge noise [26], and (iii) occupancy noise of the resident charge carrier in the QD. In order

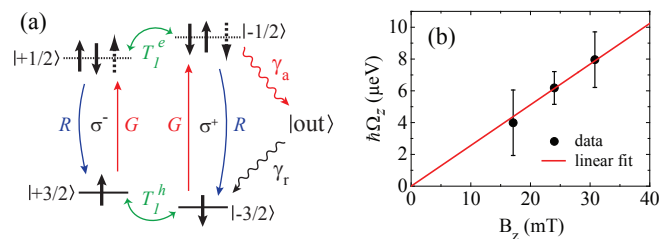


FIG. 3. (a) Sketch of the QD states and the relevant transitions. (b) Splitting of electron and hole spin states, extracted from the ratio of α and β SN power spectra, as a function of B_z .

to have a deeper insight into the particular mechanism we performed measurements of the SN power spectra as a function of the longitudinal magnetic field. These measurements show that the noise power of the β -component increases proportional to B_z which directly excludes spin splitting noise. The trion resonance frequency fluctuations can also be excluded because they are characterized by a different detuning dependence and a shorter correlation time [28]. Hence, the β -contribution is related to the occupancy noise of the QD. Note that, as it follows from symmetry arguments, the fluctuations of the hole or trion occupancy δn_h , δn_{tr} itself do not directly produce the noise of the Kerr rotation angle θ_K . However, they can produce a Kerr rotation noise in the presence of a magnetic field, $\theta_K \propto \delta n_h B_z$, $\delta n_{tr} B_z$.

Quantum dot occupancy noise arises when the average occupancy is smaller than 1. The assumption that the hole might leave the QD is well supported by the observation of the pronounced exciton transition (X^0) in the PL spectrum in Fig. 1. The correlation rate of the QD occupancy, γ_n , is determined by the rates of the transition from the trion state to an outer state and by the reoccupation of the QD by a hole, see Fig. 3(a). The ejection of the hole out of the QD can result from the Auger process. Reoccupation can either result from hole tunneling from a nearby acceptor or capture of a free hole. The origin of the measured occupancy noise is the finite Kerr rotation of an occupied QD as compared to the absence of any Kerr rotation for an empty QD in a longitudinal magnetic field at the trion resonance. The average Kerr rotation angle is

$$\theta_K \sim \frac{\gamma_1^2 - \Delta^2}{\gamma_1^2 + \Delta^2} n \Omega_z, \quad (6)$$

where $\Omega_z = \Omega_z^e - \Omega_z^h$ is the difference between electron and hole spin splittings. The average QD occupancy fluctuation squared is given by $\langle \delta n^2 \rangle = n(1-n)$ which along with Eq. (6) determines the dependence of the occupancy noise power on the detuning:

$$P_{ON,\beta}(\Delta) = A \frac{(\Gamma^2 - \Delta^2)^2}{(\Gamma^2 + \Delta^2)^4} \frac{1-n}{4} \Omega_z^2, \quad (7)$$

cf. Eq. (1). A fit to the SN power data of the β -contribution based on this equation is shown in Fig. 2(b) as gray line. We note however, that the exact shape of this dependence can be sensitive to the details of the charge dynamics in the outer states [28].

The comparison of the α and β SN power spectra as function of B_z allows by assuming $1-n \sim 1$ to estimate the spin splitting Ω_z , which is depicted in Fig. 3(b). The linear dependence on B_z additionally proves the correct identification of the origin of the β -contribution, and yields a difference of the electron and hole g -factors $|g_e - g_h| \sim 4$, which is reasonable considering the strong

renormalization of the electron and hole g -factors in In(Ga)As QDs [35, 36].

The blue dots in Fig. 2(c) depict the correlation rate of the reoccupation noise, γ_n , which decreases strongly for increasing laser detuning. This dependence has again a Lorentzian shape and is described by

$$\gamma_n = \frac{n_{tr}}{n} \gamma_a + \gamma_r, \quad (8)$$

where γ_r is the reoccupation rate. Close to the optical resonance, γ_n is dominated by the Auger recombination rate γ_a . Taking into account the saturation intensity I_0 and trion linewidth γ determined from the fit of the α -contribution we extracted the Auger rate $\gamma_a \approx 2.9 \mu\text{s}^{-1}$. This is in very good agreement with the value measured in Ref. [31] for similar QDs. For large detuning, the correlation time is not dominated by the Auger process anymore but by the reoccupation time which is slow in our sample. Our measurements of $\gamma_n(\Delta)$ yield an estimate of $\gamma_r^{-1} \sim 5 \mu\text{s}$.

In conclusion, we have measured the non-equilibrium SN of a homogeneously broadened single QD inside a microcavity in the weak coupling regime. The presented results extend SNS to the coherent single spin dynamics investigation far beyond the fluctuation-dissipation theorem which uncovers the hidden potential to study strongly non-equilibrium but yet coherent spin dynamics of the excited states and charge dynamics in the system. The SN of the strongly excited artificial atom shows two very distinct contributions. The dominant contribution is related to the optically driven heavy-hole trion transition which is potentially useful for spin-photon interfacing. This contribution shows the anticipated saturation broadening and a combined spin relaxation time resulting from the ground state (hole) and the excited state (electron in the trion). The second contribution is much weaker but may be parasitic for spin-photon interfacing. This contribution results from the intrinsic loss of the heavy hole due to the small but finite non-radiative recombination rate and the subsequent reoccupation of the QD by a hole caused by the Auger process. We expect that this reoccupation of the QD with a hole becomes slower with decreasing background doping density, i.e., QDs in unbiased structures at high background doping densities are disturbed by charge fluctuations in their surrounding and at low background doping densities by slow reoccupation.

We thank K. Pierz (PTB) for providing the sample and acknowledge the financial support by the BMBF joint research project Q.com-H (16KIS00107), the DFG (GRK 1991, OE 177/10-1), the Russian Science Foundation (No. 14-12-501067) and RF President Grant No. SP-643.2015.5.

-
- * jhuebner@nano.uni-hannover.de
† oest@nano.uni-hannover.de
- [1] A. Imamoglu, D. D. Awschalom, G. Burkard, D. P. DiVincenzo, D. Loss, M. Sherwin, and A. Small, *Phys. Rev. Lett.* **83**, 4204 (1999).
- [2] J. C. Loredo, M. A. Broome, P. Hilaire, O. Gazzano, I. Sagnes, A. Lemaitre, M. P. Almeida, P. Senellart, and A. G. White, *Phys. Rev. Lett.* **118**, 130503 (2017).
- [3] V. Giesz, N. Somaschi, G. Hornecker, T. Grange, B. Reznichenko, L. De Santis, J. Demory, C. Gomez, I. Sagnes, A. Lemaitre, O. Krebs, N. D. Lanzillotti-Kimura, L. Lanco, A. Auffèves, and P. Senellart, *Nat. Commun.* **7**, 11986 (2016).
- [4] K. De Greve, P. L. McMahon, D. Press, T. D. Ladd, D. Bisping, C. Schneider, M. Kamp, L. Worschech, S. Höfling, A. Forchel, and Y. Yamamoto, *Nat. Phys.* **7**, 872 (2011).
- [5] A. Greilich, R. Oulton, E. A. Zhukov, I. A. Yugova, D. R. Yakovlev, M. Bayer, A. Shabaev, A. L. Efros, I. A. Merkulov, V. Stavarache, D. Reuter, and A. Wieck, *Phys. Rev. Lett.* **96**, 227401 (2006).
- [6] C. Y. Hu, A. Young, J. L. O'Brien, W. J. Munro, and J. G. Rarity, *Phys. Rev. B* **78**, 085307 (2008).
- [7] C. Arnold, J. Demory, V. Loo, A. Lemaitre, I. Sagnes, M. Glazov, O. Krebs, P. Voisin, P. Senellart, and L. Lanco, *Nat. Commun.* **6**, 6236 (2015).
- [8] N. Somaschi, V. Giesz, L. De Santis, J. C. Loredo, M. P. Almeida, G. Hornecker, S. L. Portalupi, T. Grange, C. Anton, J. Demory, C. Gomez, I. Sagnes, N. D. Lanzillotti-Kimura, A. Lemaitre, A. Auffèves, A. G. White, L. Lanco, and P. Senellart, *Nat Photon* **10**, 340 (2016).
- [9] A. Dousse, J. Suffczynski, A. Beveratos, O. Krebs, A. Lemaitre, I. Sagnes, J. Bloch, P. Voisin, and P. Senellart, *Nature* **466**, 217 (2010).
- [10] T. Guerreiro, A. Martin, B. Sanguinetti, J. S. Pelc, C. Langrock, M. M. Fejer, N. Gisin, H. Zbinden, N. Sangouard, and R. T. Thew, *Phys. Rev. Lett.* **113**, 173601 (2014).
- [11] E. B. Aleksandrov and V. S. Zapasskii, *JETP* **54**, 64 (1981).
- [12] M. Oestreich, M. Römer, R. J. Haug, and D. Hägele, *Phys. Rev. Lett.* **95**, 216603 (2005).
- [13] F. Berski, H. Kuhn, J. G. Lonnemann, J. Hübner, and M. Oestreich, *Phys. Rev. Lett.* **111**, 186602 (2013).
- [14] S. A. Crooker, J. Brandt, C. Sandfort, A. Greilich, D. R. Yakovlev, D. Reuter, A. D. Wieck, and M. Bayer, *Phys. Rev. Lett.* **104**, 036601 (2010).
- [15] Y. Li, N. Sinitsyn, D. L. Smith, D. Reuter, A. D. Wieck, D. R. Yakovlev, M. Bayer, and S. A. Crooker, *Phys. Rev. Lett.* **108**, 186603 (2012).
- [16] J. Hackmann, P. Glasenapp, A. Greilich, M. Bayer, and F. B. Anders, *Phys. Rev. Lett.* **115**, 207401 (2015).
- [17] R. Dahbashi, J. Hübner, F. Berski, J. Wiegand, X. Marie, K. Pierz, H. W. Schumacher, and M. Oestreich, *Appl. Phys. Lett.* **100**, 031906 (2012).
- [18] F. Berski, J. Hübner, M. Oestreich, A. Ludwig, A. D. Wieck, and M. M. Glazov, *Phys. Rev. Lett.* **115**, 176601 (2015).
- [19] I. I. Ryzhov, G. G. Kozlov, D. S. Smirnov, M. M. Glazov, Y. P. Efimov, S. A. Eliseev, V. A. Lovtcius, V. V. Petrov, K. V. Kavokin, A. V. Kavokin, and V. S. Zapasskii, *Sci. Rep.* **6**, 21062 (2016).
- [20] F. Li and N. A. Sinitsyn, *Phys. Rev. Lett.* **116**, 026601 (2016).
- [21] A. Bechtold, F. Li, K. Müller, T. Simmet, P.-L. Ardelt, J. J. Finley, and N. A. Sinitsyn, *Phys. Rev. Lett.* **117**, 027402 (2016).
- [22] S. V. Poltavtsev, I. I. Ryzhov, M. M. Glazov, G. G. Kozlov, V. S. Zapasskii, A. V. Kavokin, P. G. Lagoudakis, D. S. Smirnov, and E. L. Ivchenko, *Phys. Rev. B* **89**, 081304 (2014).
- [23] P. Glasenapp, N. A. Sinitsyn, L. Yang, D. G. Rickel, D. Roy, A. Greilich, M. Bayer, and S. A. Crooker, *Phys. Rev. Lett.* **113**, 156601 (2014).
- [24] D. S. Smirnov, P. Glasenapp, M. Bergen, M. M. Glazov, D. Reuter, A. D. Wieck, M. Bayer, and A. Greilich, *Phys. Rev. B* **95**, 241408 (2017).
- [25] H. Horn, G. M. Müller, E. M. Rasel, L. Santos, J. Hübner, and M. Oestreich, *Phys. Rev. A* **84**, 043851 (2011).
- [26] R. Dahbashi, J. Hübner, F. Berski, K. Pierz, and M. Oestreich, *Phys. Rev. Lett.* **112**, 156601 (2014).
- [27] Since the timescale of charge fluctuations is much longer than the spin relaxation time, this has the same effect as inhomogeneous broadening in an ensemble of QDs.
- [28] See Supplemental Material for the discussion of the experimental setup, PL analysis, extraction of the Auger rate and the electron spin relaxation rate, and the theoretical model.
- [29] I. Schwartz, E. R. Schmidgall, L. Gantz, D. Cogan, E. Bordo, Y. Don, M. Zielinski, and D. Gershoni, *Phys. Rev. X* **5**, 011009 (2015).
- [30] P. Glasenapp, D. S. Smirnov, A. Greilich, J. Hackmann, M. M. Glazov, F. B. Anders, and M. Bayer, *Phys. Rev. B* **93**, 205429 (2016).
- [31] A. Kurzmann, A. Ludwig, A. D. Wieck, A. Lorke, and M. Geller, *Nano Letters* **16**, 3367 (2016).
- [32] M. M. Glazov, *JETP* **122**, 472 (2016).
- [33] V. I. Klimov, A. A. Mikhailovsky, S. Xu, A. Malko, J. A. Hollingsworth, C. A. Leatherdale, H.-J. Eisler, and M. G. Bawendi, *Science* **290**, 314 (2000).
- [34] A. L. Efros and M. Rosen, *Phys. Rev. Lett.* **78**, 1110 (1997).
- [35] T. Nakaoka, T. Saito, J. Tatabayashi, and Y. Arakawa, *Phys. Rev. B* **70**, 235337 (2004).
- [36] M. Bayer, A. Kuther, A. Forchel, A. Gorbunov, V. B. Timofeev, F. Schäfer, J. P. Reithmaier, T. L. Reinecke, and S. N. Walck, *Phys. Rev. Lett.* **82**, 1748 (1999).

Supplemental Material to “Spin and reoccupation noise beyond the fluctuation-dissipation theorem”

This supplementary information discusses the following topics:

1. Experimental setup and PL analysis
2. Extraction of the Auger rate and the electron spin relaxation rate
3. Theoretical model
 - 3.1 Model of spin and charge dynamics
 - 3.2 Separation of timescales
 - 3.3 Analysis of different probe polarization noise sources
 - 3.4 Spin noise spectrum
 - 3.5 Toy model of the outer states

S1. EXPERIMENTAL SETUP AND PL ANALYSIS

Figure S1 shows a sketch of the experimental setup. The scanning confocal microscope provides two detection arms, one for spin noise spectroscopy (SNS) and one for photoluminescence (PL) analysis. PL measurements on a quantum dot (QD) are performed prior to SNS to determine the charge state of the QD and identify the energy of

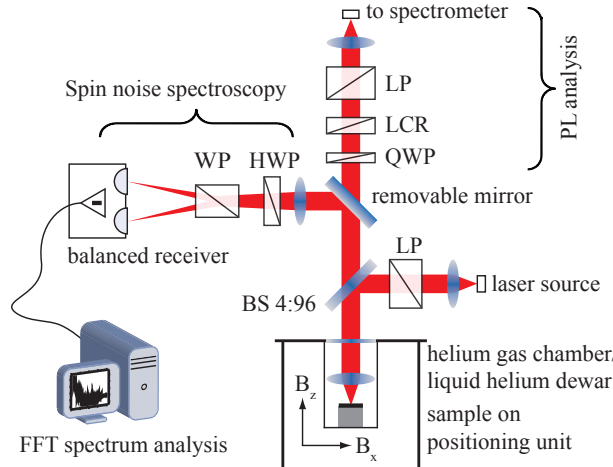


FIG. S1. Schematic of the low-temperature confocal microscope for consecutive measurements of PL and spin noise on a single QD. A beam splitter (BS) sends 4% of the incoming laser light down to the sample while 96% of the light, reflected from the sample, are transmitted for detection. The quarter waveplate (QWP), liquid crystal retarder (LCR), and linear polarizer (LP) enable polarization resolved PL measurements. A removable mirror switches between PL and SN. The half wave plate (HWP) in front of the Wollaston prism (WP) enables the exact balancing of the balanced receiver for the SN measurements.

the trion transition for SN measurements. The QD PL is analyzed with respect to the linear polarization along the two perpendicular crystal axes and spectrally resolved by a triple spectrometer with a resolution of $\approx 20 \mu\text{eV}$. Figure S2 shows the polarization-resolved PL spectrum of the QD investigated in the main text. The perpendicularly polarized PL components π_x and π_y reveal a small fine structure splitting, $\Delta_{\text{FS}} \approx 10 \mu\text{eV}$, for the high-energy transition (at about 1397.4 meV). The low-energy transition (1397.06 meV) does not show a splitting of the polarization components. The anisotropic exchange interaction leads for an uncharged QD to a splitting of the linearly polarized exciton eigenstates. Hence, the transition at higher photon energy is attributed to the neutral exciton (X^0). The absence of the fine structure splitting is an indication for a charged QD as the exchange

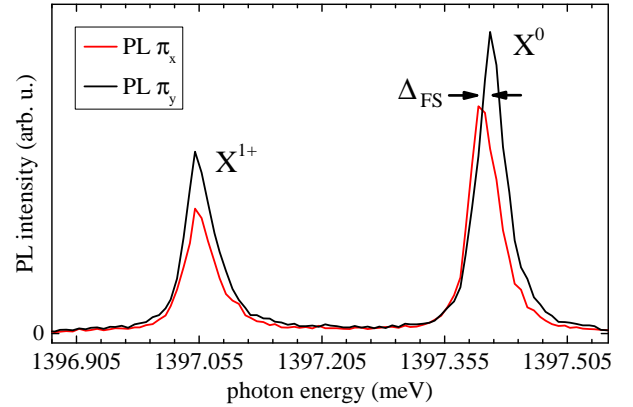


FIG. S2. Polarization-resolved photoluminescence spectrum of the QD revealing the small fine structure splitting Δ_{FS} of the exciton transition (X^0). The trion transition (X^{1+}) does not exhibit a fine structure splitting.

interaction vanishes due to the spin singlet state of the paired charge species in the trion (cf. Fig. S4). We exclude the occurrence of a negatively charged trion, due to the p-type doping of the sample, and attribute the transition at lower photon energy to the positively charged trion (X^{1+}). Spatially resolved PL measurements, the low QD density, and the statistics on other QDs ensure that both PL lines result from the same QD.

S2. EXTRACTION OF THE AUGER RATE AND THE ELECTRON SPIN RELAXATION RATE

In the main text we present the data of the correlation rates of α - and β -contribution as a function of laser detuning (cf. Fig. 2(c)). Both correlation rates, γ_s and γ_n , exhibit a Lorentzian detuning dependence with the HWHM corresponding to the trion linewidth γ_1 . The correlation rate profiles, $\gamma_s(\Delta)$ and $\gamma_n(\Delta)$, were measured for different probe laser intensities which enables the extraction of the Auger rate and electron spin relaxation rate as their impact on γ_s and γ_n increases with increasing laser intensity.

To determine the Auger rate we consider the detuning-dependent part of the β correlation rate, that is given by

$$\gamma_n(\Delta) = \frac{G}{G+R}\gamma_a, \quad (\text{S1})$$

where G and R are the generation and recombination rates associated with the trion transition. Using the relations given in the main text (see discussion around Eqs. (2)–(5)),

$$G = (\mathcal{E}^2\gamma)/(\gamma^2 + \Delta^2), \quad (\text{S2a})$$

$$R = G + \gamma_0, \quad (\text{S2b})$$

$$I/I_0 = 2\mathcal{E}^2/(\gamma\gamma_0), \quad (\text{S2c})$$

and integrating $\gamma_n(\Delta)$, we obtain the area under the Lorentzian profile as a function of laser intensity

$$A_n(I) = \frac{\pi}{2} \frac{I\gamma}{\sqrt{I_0(I+I_0)}}\gamma_a, \quad (\text{S3})$$

where γ and I_0 are the natural trion linewidth and the saturation intensity, that are determined to $\gamma = 2.2 \mu\text{eV}$ and $I_0 = 0.07 \mu\text{W}/\mu\text{m}^2$ from a fit of the measured $\gamma_1(I)$ (see Fig. 2(d) in the main text).

Figure S3 shows the area of $\gamma_n(\Delta)$ obtained from a Lorentzian fit to the measured correlation rates for each laser intensity. The fit of Eq. (S3) to these data yields the Auger rate $\gamma_a \approx 2.9 \mu\text{s}^{-1}$.

The electron spin relaxation rate is obtained in a similar way using the detuning-dependent part of the α -correlation rate

$$\gamma_s(\Delta) = \frac{G}{G+R}(\gamma_e - \gamma_h). \quad (\text{S4})$$

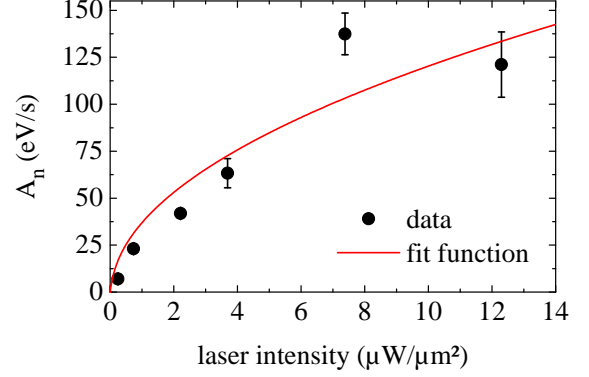


FIG. S3. The area under the measured Lorentzian profile $\gamma_n(\Delta)$ as a function of probe laser intensity. The red line is a fit according to Eq. (S3).

Here we assume $\gamma_h \sim 0$ as the hole spin relaxation is much slower than the electron spin relaxation. The integration of $\gamma_s(\Delta)$ then yields

$$A_s(I) = \frac{\pi}{2} \frac{I\gamma}{\sqrt{I_0(I+I_0)}}\gamma_e, \quad (\text{S5})$$

where again γ_e can be determined from a fit to the data of the measured Lorentzian profile $\gamma_s(\Delta)$ at different intensities, yielding $\gamma_e \approx 31 \mu\text{s}^{-1}$.

S3. THEORETICAL MODEL

S3.1. Model of spin and charge dynamics

The theoretical description of spin dynamics in a singly charged quantum dot (QD) involves at least four spin states [S1]: two heavy hole states with the spin projection $S_z^h = \pm 3/2$ on the growth axis z and the two singlet trion spin states. The trion is formed of a pair of holes in the singlet spin state and an electron with the spin projection $S_z^e = \pm 1/2$. These states are shown in Fig. S4 along with the multiple states of the resident hole outside the QD, denoted as $|\text{out}\rangle$.

The Hamiltonian of the system in an external magnetic field \mathbf{B} in the presence of the probe light has the form

$$\begin{aligned} \mathcal{H} = & \hbar\omega_0 a_{s1/2}^\dagger a_{s1/2} + \frac{\hbar}{2} (\boldsymbol{\Omega}^h \cdot \boldsymbol{\sigma})_{ss'} a_{s3/2}^\dagger a_{s'3/2} \\ & + \frac{\hbar}{2} (\boldsymbol{\Omega}^e \cdot \boldsymbol{\sigma})_{ss'} a_{s1/2}^\dagger a_{s'1/2} + \left(\hbar\mathcal{E}_s e^{-i\omega t} a_{s1/2}^\dagger a_{s3/2} + \text{h.c.} \right). \end{aligned} \quad (\text{S6})$$

Here the summation over the repeated indices $s, s' = \pm$ is assumed, $a_{\pm 3/2}$, $a_{\pm 1/2}^\dagger$ are the annihilation and creation operators for the resident hole, $a_{\pm 1/2}$, $a_{\pm 1/2}^\dagger$ are

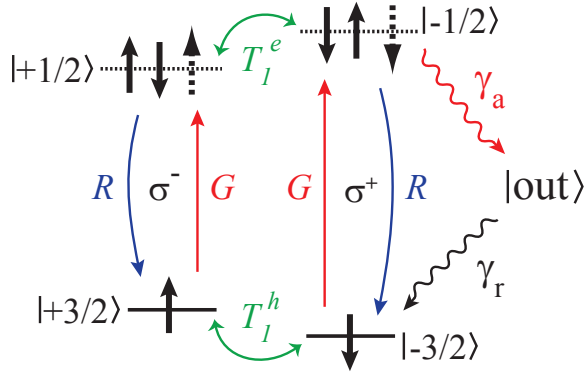


FIG. S4. The sketch of the QD and outer states and transitions between them.

the corresponding operators of the trion, ω_0 is the trion resonance frequency, $\mathbf{\Omega}^{e(h)} = \mu_B \hat{g}^{e(h)} \mathbf{B} / \hbar$ is the electron (hole) Larmor precession frequency with $\hat{g}_{e(h)}$ being the corresponding tensors of g -factors, $\boldsymbol{\sigma}$ is the vector composed of Pauli matrices, and \mathcal{E}_{\pm} are the trion optical transition matrix elements in σ^{\pm} polarizations, respectively, being the product of the corresponding electric field component amplitude in the QD and the transition dipole moment. We consider the weak coupling regime, so the electromagnetic field inside the microcavity can be treated classically.

The Hamiltonian accounts for the coherent processes, e.g. Rabi oscillations between hole and trion states. The incoherent processes, which are shown in Fig. S4, should be treated in the density matrix formalism:

$$\dot{\rho}(t) = i[\rho(t), \mathcal{H}] - \mathcal{L}\{\rho(t)\}. \quad (\text{S7})$$

Here $\rho(t)$ is the density matrix of the system, the dot denotes the time derivative, and the Lindblad superoperator describes the spin relaxation, recombination and reoccupation processes. The charge and spin dynamics in the system are described by the set of coupled equations for the expectation values of operators O :

$$\langle O \rangle = \text{Tr}[O\rho(t)]. \quad (\text{S8})$$

In the longitudinal magnetic field this system reads:

$$\dot{n}_h = 2\mathcal{E}d_x'' + \gamma_0 n_{\text{tr}} + \gamma_r n_{\text{out}}, \quad (\text{S9a})$$

$$\dot{n}_{\text{tr}} = -2\mathcal{E}d_x'' - \gamma_0 n_{\text{tr}} - \gamma_a n_{\text{tr}}, \quad (\text{S9b})$$

$$\dot{\sigma}_h = -2\mathcal{E}d_y' - \frac{1}{T_1^h} \sigma_h + \gamma_0 \sigma_{\text{tr}}, \quad (\text{S9c})$$

$$\dot{\sigma}_{\text{tr}} = 2\mathcal{E}d_y' - \frac{1}{T_1^e} \sigma_{\text{tr}} - \gamma_0 \sigma_{\text{tr}} - \gamma_a \sigma_{\text{tr}}, \quad (\text{S9d})$$

$$\dot{d}_x' = -\Delta d_x'' - \Omega d_y''/2 - \gamma d_x', \quad (\text{S9e})$$

$$\dot{d}_x'' = \mathcal{E}(n_{\text{tr}} - n_h)/2 + \Delta d_x' - \Omega d_y''/2 - \gamma d_x'', \quad (\text{S9f})$$

$$\dot{d}_y' = \mathcal{E}(\sigma_h - \sigma_{\text{tr}})/2 - \Delta d_y'' + \Omega d_x'/2 - \gamma d_y', \quad (\text{S9g})$$

$$\dot{d}_y'' = \Delta d_y' + \Omega d_x''/2 - \gamma d_y''. \quad (\text{S9h})$$

Here $n_h = \langle a_{+3/2}^\dagger a_{+3/2} + a_{-3/2}^\dagger a_{-3/2} \rangle$ and $n_{\text{tr}} = \langle a_{+1/2}^\dagger a_{+1/2} + a_{-1/2}^\dagger a_{-1/2} \rangle$ are the populations of the QD ground state and the trion state, respectively. Similarly $\sigma_h = \langle a_{+3/2}^\dagger a_{+3/2} - a_{-3/2}^\dagger a_{-3/2} \rangle$ and $\sigma_{\text{tr}} = \langle a_{+1/2}^\dagger a_{+1/2} - a_{-1/2}^\dagger a_{-1/2} \rangle$ are the z spin polarizations of the corresponding states. $\Omega = \Omega_z - \Omega_z^h$ is the total spin splitting of the optical transitions in σ^+ and σ^- polarizations. The quantities proportional to the components dipole moment are defined in the canonical basis [S2] as

$$d_x = \frac{-d_+ + d_-}{\sqrt{2}}, \quad d_y = -i \frac{d_+ + d_-}{\sqrt{2}}, \quad (\text{S10})$$

where $d_{\pm} = \langle a_{\pm 3/2}^\dagger a_{\pm 1/2} \rangle$ and one or two primes in Eqs. (S9) denote the real or imaginary parts of the corresponding expectation values, respectively. Finally we consider linearly polarized probe light, so that $\mathcal{E}_{\pm} = \mp \mathcal{E} / \sqrt{2}$ with \mathcal{E} being a real constant. Therefore the dipole moment components denoted by one prime are in phase with the probe beam, and two primes stands for the component shifted by 90° . The Faraday and ellipticity signals are proportional, respectively to d_y'' and d_y' [S3].

In Eqs. (S9) we introduce the hole and trion spin relaxation rates T_1^h and T_1^e , respectively, and assume, that the nuclear spins are effectively decoupled from the hole and electron spins due to the strong magnetic field [S4], so the hyperfine interaction can be included in the phenomenological hole and trion spin relaxation rates [S5]. The trion recombination rate, unrelated to the cavity photon emission, is denoted as γ_0 . The Auger process leads to the recombination of the trion accompanied by the escape of the hole from the QD with the rate γ_a . Finally γ_r stands for the recharging of the QD, i.e. it is the rate of transitions from the outer states to the hole ground state in the QD. The spin relaxation in the outer states is assumed to be very fast, so that the hole returns to the QD spin unpolarized. The direct transitions from the QD ground state to the outer states are neglected because of the strong spatial confinement. The hole-trion dephasing rate is denoted as γ . It is in general case greater or equal to $(\gamma_0 + \gamma_a)/2 + 1/T_2^h + 1/T_2^e$ with $T_2^{h,e}$ being the hole and trion transverse spin relaxation rates.

The system of Eqs. (S9) is not complete, because one has to consider also the charge dynamics in the outer states. The parameter n_{out} in Eq. (S9a) describes the occupancy of some outer states with the average reoccupation rate γ_r . In principle there could be multiple outer states with different transition rates to the QD ground state. Moreover, transitions between the outer states can take place as well. In this paper we do not study the charge dynamics outside the quantum dot. The simplest model, assuming a single outer state is discussed in Sec. S3.5.

S3.2. Separation of timescales

In the typical QD systems, and in particular in the sample under study, the trion generation and recombination are much faster, than all the other timescales. This means that during the time $\sim \gamma_0^{-1}$ the quasi-equilibrium is established with respect to the generation and recombination processes. This quasi steady state parametrically depends on the total QD population $n = n_h + n_{tr}$ and the total spin $S_z = (\sigma_h + \sigma_{tr})/2$. These quantities are preserved during the trion generation and recombination, and their dynamics are described by slow spin relaxation and Auger processes.

Hence, from Eq. (S9) under the experimentally relevant assumptions

$$\gamma_0, \Delta \gg \Omega, \gamma_e, \gamma_h, \gamma_a, \gamma_r \quad (\text{S11})$$

one finds that in the quasi steady state (c.f. Eq. (3))

$$\frac{n_{tr}}{n} = \frac{\sigma_{tr}}{2S_z} = \frac{G}{G+R}, \quad (\text{S12})$$

where we have introduced the generation rate G (Eq. (2)) and the recombination rate $R = \gamma_0 + G$. Note that in the limit $\mathcal{E} \rightarrow 0$ the generation rate vanishes and $R = \gamma_0$.

S3.3. Analysis of different probe polarization noise sources

The Faraday rotation is determined by the component of the dipole moment d''_y . In the quasi steady state it can be presented as

$$d''_y = \frac{\mathcal{E}\Delta}{\gamma_1^2 + \Delta^2} S_z + \frac{\mathcal{E}(\gamma_1^2 - \Delta^2)}{4(\gamma_1^2 + \Delta^2)^2} n\Omega, \quad (\text{S13})$$

where $\gamma_1 = \gamma\sqrt{1 + 2\mathcal{E}^2/(\gamma\gamma_0)}$ (cf Eq. (5) in the main text) is the trion linewidth renormalized by the saturation broadening effect. From this expression one can see, that the Faraday rotation can be induced by (i) hole or trion spin polarization and (ii) longitudinal magnetic field.

Experimentally the spin noise is studied in reflection geometry. The rotation of the polarization plane of the reflected light (Kerr rotation) can be in principle contributed by the dipole moment components d''_y and d''_x as well, depending on the position of the QD inside the cavity and the thickness of the cap layer [S3]. Indeed we have observed somewhat different SN power spectra for different QDs. In this paper we focus mainly on a particular QD, where the Kerr rotation profile is consistent with the analysis of d''_y as for the Faraday rotation.

Analysis of Eq. (S13) reveals multiple possible sources of Kerr rotation fluctuations and yields the corresponding SN power spectra.

The first source is the spin noise. The corresponding SN power spectrum is

$$(\delta\theta_K^2)_{SN} \sim \left(\frac{2\mathcal{E}\Delta}{\gamma_1^2 + \Delta^2} \right)^2 \langle \delta S_z^2 \rangle_0, \quad (\text{S14})$$

cf. Eq. (1) of the main text. The angular brackets with the subscript 0 denote the quantum mechanical average with the steady state density matrix, or equivalently the temporal average. Eq. (S14) describes the usual spin-induced Kerr rotation noise profile [S6], characterized by the dip exactly at the trion resonance, $\Delta = 0$. This contribution describes the α -contribution in the observed spectra. We note that

$$\langle \delta S_z^2 \rangle_0 = \bar{n}/4, \quad (\text{S15})$$

where $\bar{n} \equiv \langle n \rangle_0$ is the average steady state QD occupancy, which in principle also depends on the detuning and the probe power. This dependence is determined by the Auger process, as well as by the transitions between outer states and the reoccupation process. Detailed description of this dynamics is beyond the scope of the present study, and since this dependence does not qualitatively change the shape of the SN power spectrum, we phenomenologically describe the spectrum by Eq. (1) of the main text, where the parameter Γ can be different from γ_1 . The simplest model describing the renormalization of γ_1 is presented in Sec. S3.5.

The QD occupation noise also gives rise to the Kerr rotation fluctuations as

$$(\delta\theta_K^2)_{ON} \sim \frac{\mathcal{E}^2(\gamma_1^2 - \Delta^2)^2}{4(\gamma_1^2 + \Delta^2)^4} \Omega^2 \langle \delta n^2 \rangle_0. \quad (\text{S16})$$

This contribution appears only in the presence of the longitudinal magnetic field. Moreover, it requires that there is a nonzero average of QD occupancy fluctuation $\langle \delta n^2 \rangle_0$, i.e., a finite probability to find the QD in the empty state. This contribution is maximum at the trion resonance and the dependence on the probe frequency is similar to a Gaussian profile. The QD occupancy fluctuations are responsible for the β -contribution in the observed spectra. The dependence of $\langle \delta n^2 \rangle_0 = \bar{n}(1 - \bar{n})$ on the detuning

and renormalization of γ_1 in this contribution are also discussed in Sec. S3.5.

For the sake of completeness we present the other possible contributions to the Kerr rotation noise. The nuclear spin fluctuations give rise to the additional splitting $\delta\Omega_n$ of the trion transitions in σ^+ and σ^- polarizations [S7]. The nuclear induced Kerr rotation noise power is given by

$$(\delta\theta_K^2)_{NSN} \sim \frac{\mathcal{E}^2(\gamma_1^2 - \Delta^2)^2}{4(\gamma_1^2 + \Delta^2)^4} \bar{n} \langle \delta\Omega_n^2 \rangle_0. \quad (\text{S17})$$

This contribution is characterized by the same dependence on the detuning as $(\delta\theta_K^2)_{ON}$, but (i) does not depend on the magnitude of the external magnetic field in contrast to the results presented in the main text and (ii) has typically a smaller amplitude. Indeed the typical spin splitting induced by the Overhauser field is $\sim 0.5 \mu\text{eV}$, while in the applied magnetic field $B_z = 31 \text{ mT}$ the spin splitting is expected to be a bit larger. Therefore we conclude that this contribution is not observed in our experiment.

The charge noise in the environment of the QD leads to the fluctuations of the resonance frequency ω_0 , and as a result to fluctuations of the detuning Δ . This in turn leads to the fluctuations of both terms in Eq. (S13). The corresponding contribution to the SN power spectrum reads

$$(\delta\theta_K^2)_{CN} \sim \left[\frac{(2\mathcal{E})^2(\gamma_1^2 - \Delta^2)^2}{(\gamma_1^2 + \Delta^2)^4} \langle S_z^2 \rangle_0 + \frac{(\mathcal{E}\Delta)^2(3\gamma_1^2 - \Delta^2)^2}{(\gamma_1^2 + \Delta^2)^6} \Omega^2 \bar{n} \right] \langle \delta\omega_0^2 \rangle_0. \quad (\text{S18})$$

The first line of this expression gives rise to the same SN power spectrum, as $(\delta\theta_K^2)_{ON}$ and $(\delta\theta_K^2)_{NSN}$, but it requires the presence of spin fluctuations, $\langle S_z^2 \rangle_0$. Therefore the corresponding correlation time can not be longer than the spin relaxation time. Since experimentally the correlation time of the β -component is longer than that of the α -component, we conclude that this contribution was not observed. Finally, the second line of Eq. (S18) describes the contribution to Kerr rotation noise, which has a dip at zero detuning. Hence, it is inconsistent with the observed β -contribution SN power spectrum. The fact that the charge noise in the surrounding of the quantum dot does not provide additional contribution to the SN power spectra is also supported by the observation of the SN power spectrum $(\delta\theta_K^2)_{SN}$, with the dip at the QD resonance, in contrast to Ref. [S8].

S3.4. Spin noise spectrum

In the previous subsection we have shown, that α and β -contributions to the Kerr rotation noise are related to the spin and QD occupation fluctuations, respectively. In

order to describe the corresponding SN frequency spectra we consider slow dynamics of S_z and n assuming that the quasi-equilibrium is established with respect to the generation and recombination processes in the QD, as described in the main text.

Taking into account Eq. (S12) one finds from Eqs. (S9c) and (S9d)

$$\dot{S}_z = -\gamma_s S_z, \quad (\text{S19})$$

where γ_s is given by Eq. (4) of the main text. In order to find the SN frequency spectrum we apply the Langevin method [S9 and S10]. The spin fluctuation obeys the equation

$$\delta\dot{S}_z(t) + \gamma_s \delta S_z(t) = \xi_s(t), \quad (\text{S20})$$

where the Langevin force $\xi_s(t)$ is described by the correlator

$$\langle \xi_s(t) \xi_s(t') \rangle_0 = 2\gamma_s \langle \delta S_z^2 \rangle_0 \delta(t - t'). \quad (\text{S21})$$

This equation along with Eq. (S15) yields the spin noise spectrum

$$\langle \delta S_z^2 \rangle = \frac{\bar{n}}{2} \frac{\gamma_s}{\gamma_s^2 + \omega^2}. \quad (\text{S22})$$

Hence, the SN frequency spectrum, as usual, has the form of a Lorentzian, centered at zero frequency and has a HWHM equal to γ_s .

Similarly the slow dynamics of QD population are described by

$$\dot{n} = -\frac{G\gamma_a}{R+G}n + \gamma_r n_{out}, \quad (\text{S23})$$

where we have used Eqs. (S9a), (S9b) and (S12). We recall, that n_{out} is the population of the states, which predominantly contribute to the QD reoccupation. Therefore in order to describe the charge dynamics in the QD one has to adopt some model of the outer states.

S3.5. Toy model of the outer states

The detailed investigation of charge dynamics outside the QD is beyond the scope of this paper. In this section we present the simplest model, in which all the outer states are reduced to one quantum level, and demonstrate the qualitative consequences of QD emptying and reoccupation dynamics.

Provided all the outer states are reduced to a single state, its population satisfies the equation

$$\dot{n}_{out} = \gamma_a n_{tr} - \gamma_r n_{out}, \quad (\text{S24})$$

and the particle conservation states that $n_{out} = 1 - n$. Taking into account Eq. (S23) one finds the steady-state QD occupancy

$$\bar{n} = \frac{\gamma_r(G+R)}{\gamma_r(G+R) + \gamma_a G}. \quad (\text{S25})$$

When Auger recombination is slow, $\gamma_a \ll \gamma_r$, the population is unity independent on the generation and recombination rates. In realistic systems the opposite limit is realized, $\gamma_a \gg \gamma_r$ [S11], in which even a small excitation $G \sim R(\gamma_r/\gamma_a)$ leads to the efficient emptying of the QD.

Substituting Eq. (S25) into Eqs. (S14) and (S16) one obtains the following SN power spectra

$$(\delta\theta_K^2)_{SN} \sim \frac{2(\mathcal{E}\Delta)^2}{(\gamma_1^2 + \Delta^2)(\gamma_2^2 + \Delta^2)}, \quad (\text{S26})$$

$$(\delta\theta_K^2)_{ON} \sim \frac{(\mathcal{E}^2\Omega)^2(\gamma_2^2 - \gamma_1^2)(\gamma_1^2 - \Delta^2)^2}{4(\gamma_1^2 + \Delta^2)^3(\gamma_2^2 + \Delta^2)^2}, \quad (\text{S27})$$

where we have introduced

$$\gamma_2 = \sqrt{\gamma_1^2 + \frac{\gamma_a\gamma\mathcal{E}^2}{\gamma_r\gamma_0}}. \quad (\text{S28})$$

In general case one can see that $\gamma_2 > \gamma_1$. Therefore Eqs. (S26) and (S27) describe the SN power spectra with the characteristic width larger than γ_1 because of the fast Auger recombination. The physical reason for the broadening is the fast emptying of the QD for small generation rates, which leads to the strong suppression of spin noise at small detunings and the enhancement of the relative contribution at large detunings.

We find that the presented toy model does not quantitatively describe the observed SN power spectra. Therefore we describe the spin noise power spectra by the expressions Eqs. (1) and (7) of the main text, which can be obtained from Eqs. (S14) and (S16) by the phenomenological renormalization of γ_1 to Γ .

Note that, despite the charge dynamics outside the QD significantly modify the SN power spectra, they do not affect the width of the SN frequency spectra, Eqs. (4) and (8). Indeed the spin relaxation rate is obtained in Sec. S3.4 without any assumptions about outer states and the occupancy fluctuations are described by

$$\dot{\delta n}(t) + \gamma_n \delta n(t) = \xi_n(t), \quad (\text{S29})$$

where γ_n is given by Eq. (8). Although the second term in Eq. (8) depends on the model of dynamics in outer states, the main contribution, given by the first term is not dependent on these dynamics. As one can see in Fig. 2(c), the Auger related contribution to the occupancy correlation time dominates at small detunings. We recall that in the Langevin method the random force $\xi_n(t)$ satisfies

$$\langle \xi_n(t)\xi_n(t') \rangle_0 = 2\gamma_n \langle \delta n^2 \rangle_0 \delta(t-t'), \quad (\text{S30})$$

and is introduced formally in order to support the average of squared fluctuation $\langle \delta n^2 \rangle_0$.

Therefore the increase of the rates γ_s and γ_n is described by the Lorentzian profile with the HWHM given by γ_1 independent on the dynamics in outer states. This fact allows for the reliable measurement of hole and trion spin relaxation times, as well as the Auger rate, demonstrated in this Letter.

* jhuebner@nano.uni-hannover.de

† oest@nano.uni-hannover.de

- [S1] M. M. Glazov, *JETP* **122**, 472 (2016).
- [S2] D. A. Varshalovich, A. N. Moskalev, and V. K. Khersonskii, *Quantum theory of angular momentum* (World scientific, Singapore, 1988).
- [S3] I. A. Yugova, M. M. Glazov, E. L. Ivchenko, and A. L. Efros, *Phys. Rev. B* **80**, 104436 (2009).
- [S4] P. Glasenapp, D. S. Smirnov, A. Greilich, J. Hackmann, M. M. Glazov, F. B. Anders, and M. Bayer, *Phys. Rev. B* **93**, 205429 (2016).
- [S5] M. M. Glazov, *Phys. Rev. B* **91**, 195301 (2015).
- [S6] V. S. Zapasskii, A. Greilich, S. A. Crooker, Y. Li, G. G. Kozlov, D. R. Yakovlev, D. Reuter, A. D. Wieck, and M. Bayer, *Phys. Rev. Lett.* **110**, 176601 (2013).
- [S7] F. Berski, J. Hübner, M. Oestreich, A. Ludwig, A. D. Wieck, and M. M. Glazov, *Phys. Rev. Lett.* **115**, 176601 (2015).
- [S8] R. Dabhashi, J. Hübner, F. Berski, K. Pierz, and M. Oestreich, *Phys. Rev. Lett.* **112**, 156601 (2014).
- [S9] L. D. Landau and E. M. Lifshitz, *Statistical Physics, Part 1* (Butterworth-Heinemann, Oxford, 2000).
- [S10] M. M. Glazov and E. L. Ivchenko, *Phys. Rev. B* **86**, 115308 (2012).
- [S11] A. Kurzmann, A. Ludwig, A. D. Wieck, A. Lorke, and M. Geller, *Nano Letters* **16**, 3367 (2016).